Soft Matter

Accepted Manuscript

ROYAL SOCIETY OF CHEMISTRY

www.rsc.org/softmatter

While a high cholesterol concentration of 40mol% cholesterol led to the formation of immiscible cholesterol bilayers in saturated lipid membranes, the addition of ASA was found to significantly increase the fluidity of the bilayers and to dissolve the cholesterol patches.

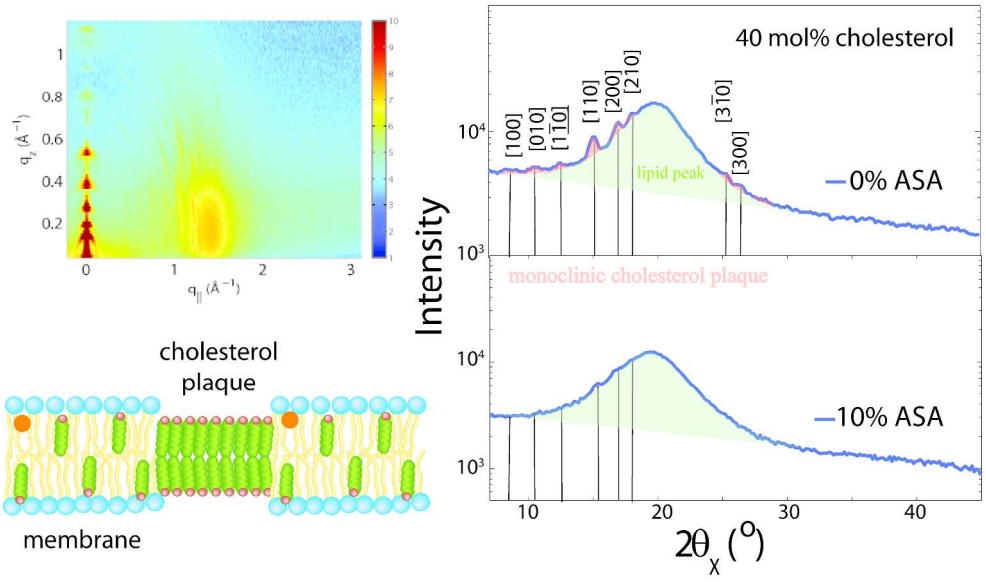

328x189mm (300 x 300 DPI)

Acetylsalicylic Acid (ASA) Increases the Solubility of Cholesterol When Incorporated in Lipid Membranes

Richard J. Alsop,[1] Matthew A. Barrett,[1] Songbo Zheng,[1] Hannah Dies,[1] and Maikel C. Rheinstädter[1,2,*]

[1] *Department of Physics and Astronomy, McMaster University, Hamilton, ON, Canada*
[2] *Canadian Neutron Beam Centre, National Research Council Canada, Chalk River, ON, Canada*

(Dated: April 7, 2014)

Cholesterol has been well established as a mediator of cell membrane fluidity. By interacting with lipid tails, cholesterol causes the membrane tails to be constrained thereby reducing membrane fluidity, well known as the condensation effect. Acetylsalicylic acid (ASA), the main ingredient in Aspirin, has recently been shown to increase fluidity in lipid bilayers by primarily interacting with lipid head groups. We used high-resolution X-ray diffraction to study both ASA and cholesterol coexisting in model membranes of dimyristoylphosphatidylcholine (DMPC). While a high cholesterol concentration of 40 mol% cholesterol led to the formation of immiscible cholesterol bilayers, as was reported previously, increasing the amount of ASA in the membranes between 0 to 12.5 mol% was found to significantly increase the fluidity of the bilayers and dissolve the cholesterol plaques. We, therefore, present experimental evidence for an interaction between cholesterol and ASA on the level of the cell membrane at elevated levels of cholesterol and ASA.

Keywords: lipid bilayers containing cholesterol, lipid bilayers containing ASA, cholesterol-ASA interaction in membranes, membrane fluidity, Low-Dose-Aspirin-Therapy, molecular structure, X-ray diffraction

1. INTRODUCTION

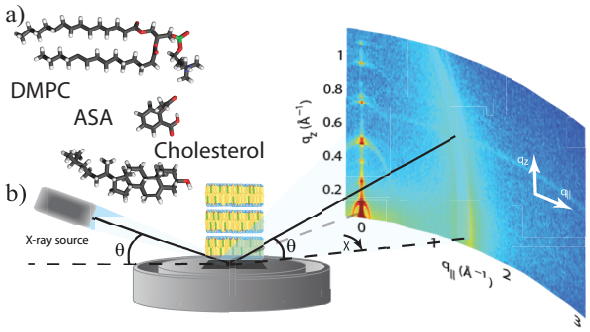

FIG. 1. a) Lipid, ASA and cholesterol molecule. b) Schematic diagram of the X-ray scattering experiment. The in-plane and out-of-plane structure of the membranes was determined from 2-dimensional intensity maps. Highly oriented multi lamellar membranes were prepared. 2θ and $2\theta\chi$ are the out-of-plane respective in-plane diffraction angles.

The biological membrane is a complex structure, composed of various lipid species, sterols, proteins, and other small molecules. An important consequence arising from the complexity of the structure is fluidity[1–3]. By being fluid, the structure allows for fast diffusion of small molecules and lateral diffusion of membrane proteins[4]. The fluidity of a membrane also determines its bending modulus, and ability to form pores[5,6]. Cholesterol, with its stiff hydrocarbon ring structure, is known to increase membrane rigidity acting as a physiological mediator of membrane fluidity. The liquid-ordered (l_o) phase, which is observed at high concentrations of cholesterol[7], was reported to combine the properties of gel and fluid phases, in other words, it is as well ordered as the gel phase, but 'softer' than the fluid phase[8,9], with smaller viscosity and restoring forces. In addition, cholesterol is speculated to be un-evenly distributed in the membrane. Regions with high cholesterol among a larger membrane are labeled lipid rafts[10], which are often implicated in cell signalling and neuro-transmission, among other roles[10–21].

However, a high concentration of cholesterol causes a disadvantageous decrease in fluidity and a change in homeostasis, leading to reduced health of the individual. Possible effects of high cholesterol include high blood pressure and hypertension. As well, high cholesterol serves as a risk factor for myocardial infarctions. Biochemical and physiological studies have allowed for the discovery of many pharmaceuticals to specifically lower cholesterol levels, along with medications to reduce the symptoms and effects of high cholesterol. A common treatment for the primary and secondary prevention of myocardial events, in patients with high cholesterol, is the daily intake of the analgesic Aspirin (acetylsalicylic acid, ASA) as part of a regimen known as Low-Dose Aspirin Therapy[22–24].

Despite progress in the treatment of high cholesterol, explaining and mitigating the adverse effects of cholesterol is still a rich area. In particular, the field of membrane biophysics has proven effective in explaining and quantifying the effects of cholesterol in the context of model membrane systems. X-Ray and neutron scattering experiments have been able to probe the position of cholesterol within the membrane and quantify and understand the effects of cholesterol[3,8,9,25–35]. The hydrophobic cholesterol molecule partitions itself in the hydrophobic membrane core. In saturated lipid bilayers, the

cholesterol molecules are known to align parallel to the lipid acyl chains, well known umbrella-model[34,36]. In the umbrella model each lipid molecule is associated with two cholesterol molecules, which cause the membrane tails to be constrained, suppress lipid tail fluctuations thereby increasing membrane thickness and reducing membrane fluidity. The lipid head group is thought to act as an 'umbrella', which protects the hydrophobic part of the cholesterol molecules from the aqueous environment. In highly unsaturated membranes, cholesterol was found to reside also in the centre of the membranes[28,37]. Small, transient cholesterol domains at physiological cholesterol levels were recently reported from computer simulations[38] and experiments[35]. At high concentrations of cholesterol, above ∼40 mol%, immiscible cholesterol bilayers may form sponatneously.[39–45].

ASA was found to incorporate in lipid membranes and to primarily interact with the head groups, increasing lipid fluidity[46]. Aspirin and other non-steroidal anti-inflammatory drugs (NSAID's) are able to interact with lipid membranes leading to increased bending ability and pore formation in real and model membranes[47–49]. However, given the opposing effects of ASA and cholesterol in the membrane, a direct interaction has never been investigated.

We investigated DMPC membranes containing varied amounts of cholesterol and ASA using high-resolution X-ray diffraction. Lamellar stacks of bilayers containing ASA, cholesterol, and the saturated phospholipid dimyristoylphosphocholine (DMPC) were prepared. Samples contained up to 12.5 mol% ASA and 40 mol% cholesterol. We used 2-dimensional X-ray diffraction, covering large areas of reciprocal space, to probe the in-plane and out-of-plane structure of the membranes in their liquid-ordered phase. We find experimental evidence for an interaction between cholesterol and ASA.

2. MATERIALS AND METHODS

2.1. Preparation of the Highly-Oriented Multi-Lamellar Membrane Samples

Highly oriented multi lamellar membranes were prepared on single-side polished silicon wafers. 100 mm diameter, 300 μm thick silicon (100) wafers were precut into 2×2 cm^2 chips. 1,2-dimyristoyl-sn-glycero-3-phosphocholine (DMPC, $C_{36}H_{72}NO_8P$), acetylsalicylic acid (ASA, $C_9H_8O_4$) and cholesterol ($C_{27}H_{46}O$), as depicted in Figure 1 a), were mixed in different ratios and dissolved in a 1:1 chloroform/2,2,2-trifluoroethanol (TFE) solution at a concentration of 15 mg/ml.

The lipid solution did not spread well on ultrasonic-cleaned wafers and de-wetted during drying. The silicon substrates were, therefore, cleaned in a piranha acid solution made of 98% concentrated H_2SO_4 and 30% concentrated H_2O_2 at a ratio of 3:1 by volume. Wafers were placed in this solution, covered with parafilm and kept at 298 K for 30 minutes. This treatment removes all organic contamination and leaves the substrates in a hydrophilic state. The 1:1 mix of chloroform/TFE, which was used to dissolve lipids and chloroform, is a non-polar solvent. In order for the solvent to spread well and cover the whole substrate uniformly, the silicon wafers were made hydrophobic to match the solvent properties. We used silanization to cover the silicon surface through self-assembly with organo-functional alkoxysilane molecules (APTES). The organic part of the APTES molecules was found to provide a perfect hydrophobic interface for the formation of the biological tissue[39,46].

A 1% (by volume) solution of APTES and 99% ethanol was prepared. A 1 mL syringe was filled with 0.2 mL of dry nitrogen. This nitrogen was ejected into 99% APTES, and 0.2 mL of APTES was drawn into the syringe. This syringe is then submerged in 19.8 mL of ethanol before ejecting the APTES. The wafers were immersed in the APTES solution and covered with parafilm, kept at 298 K and placed on a tilting incubator (20 speed, 3 tilt) for 12 hours. The tilting incubator creates a circular flow in the beaker to ensure an even APTES distribution and prevent buildup on the surface of the wafers. The wafers were then placed in a clean pyrex dish and annealed in vacuum at 388 K for 3 hours to create a uniform coverage of the APTES molecules on the surface[50].

Each wafer was thoroughly rinsed three times by alternating with ∼50 mL of ultra pure water and methanol. The methanol was cleaned using a 0.2 μm filter before use to avoid surface contamination. The tilting incubator was heated to 313 K and the lipid solution was placed inside to equilibrate. The wafers were rinsed in methanol, dried with nitrogen gas and placed in the incubator. 200 μL of lipid solution was applied on each wafer and the wafers were covered with a petri dish to let the solvent evaporate slowly during a period of ∼15 minutes. The slow drying allows time for the lamellar membranes to form on the substrate. Wafers were tilted during the drying process for 30 minutes (speed 15, tilt 1) such that the lipid solution spread evenly on the wafers.

After drying, the samples were placed in vacuum at 313 K for 12 hours to remove all traces of the solvent. The bilayers were annealed and rehydrated before use in a saturated K_2SO_4 solution which provides ∼98% relative humidity (RH). The hydration container was allowed to equilibrate at 293 K in an incubator. The temperature of the incubator was then increased gradually from 293 K to 303 K over a period of ∼5 hours to slowly anneal the multi lamellar structure.

This procedure results in highly oriented multi lamellar membrane stacks and a uniform coverage of the silicon substrates. About 3,000 highly oriented stacked membranes with a total thickness of ∼10 μm are produced using this protocol. The samples were stored in a refrigerator at 5°C and heated to 55°C for 1 h before scanning to erase a possible thermal history. This procedure in particular destroys possible crystalline L_C or sub-gel

phases that may form during storage at low temperatures and low hydration[51].

The high sample quality and high degree of order is a prerequisite to determine the in-plane structure of the membranes and the arrangement of cholesterol and ASA molecules. Table 1 lists all samples prepared for this study.

2.2. X-ray scattering experiment

X-ray diffraction data was obtained using the Biological Large Angle Diffraction Experiment (BLADE) in the Laboratory for Membrane and Protein Dynamics at McMaster University. BLADE uses a 9 kW (45 kV, 200 mA) CuKα rotating anode at a wavelength of 1.5418 Å. Both source and detector are mounted on movable arms such that the membranes stay horizontal during the measurements. Focussing multi-layer optics provides a high intensity parallel beam with monochromatic X-ray intensities up to 10^{10} counts/(s $\times$ mm^2). This beam geometry provides optimal illumination of the solid supported membrane samples to maximize the scattering signal.

A sketch of the scattering geometry is shown in Figure 1 b). By using highly oriented membrane stacks, the lateral in-plane ($q_{||}$) and out-of-plane (q_z) structure of the membranes could be determined with sub-nanometer resolution. A point detector was used in combination with slits and collimators in front and after the samples to optimize the signal-to-noise-ratio. The detector was moved along a spherical surface around the sample, as defined by the two angles 2θ and $2\theta\chi$. The result of such an X-ray experiment is a 2-dimensional intensity map of a large area (0.03 Å^{-1} $< q_z <$1.1 Å^{-1} and 0 Å^{-1} $< q_{||} <$3.1 Å^{-1}) of the reciprocal space, as sketched in Figure 1 b). This information was used to develop the molecular structure of the membrane samples.

All scans were measured at 20°C and 50% RH, in the gel phase of the bilayers[52,53]. Fully hydrated liquid-crystalline samples are generally assumed to best mimic physiologically relevant conditions[31,54]. However, these disordered bilayers do not diffract well (i.e. give rise to a limited number of quasi-Bragg peaks), and as such do not lend themselves ideally to traditional crystallographic analysis. In order to obtain high resolution diffraction data, the membranes in this study were measured below the gel-fluid transition temperature of T=296.6 K in multi-lamellar DMPC systems[55,56] and at a reduced hydration. As high resolution structural data are needed to determine the location of the different molecular components, this protocol permits the measurement of high order Bragg peaks, and thereby achieve a high spatial resolution, as demonstrated by Hristova and White[57]. Consequently, the membranes were in their gel (L_β) phase[33,52,53]. All conclusions drawn, therefore, refer to this phase state of the system.

2.3. The Calculation of Electron Densities

The out-of-plane structure of the membranes was determined using specular reflectivity, see, for instance,[31,54] for recent reviews. The electron density, $\rho(z)$, is approximated by a 1-dimensional Fourier analysis[58]:

$$\rho(z) = \rho_W + \frac{F(0)}{d_z} + \frac{2}{d_z}\sum_{n=1}^{N} F(q_n)\nu_n \cos(q_n z)$$
$$= \rho_W + \frac{F(0)}{d_z} + \frac{2}{d_z}\sum_{n=1}^{N} \sqrt{I_n q_n}\nu_n \cos\left(\frac{2\pi n z}{d_z}\right). \quad (1)$$

N is the highest order of the Bragg peaks observed in the experiment and ρ_W the electron density of bulk water. The integrated peak intensities, I_n, are multiplied by q_n to receive the form factors, $F(q_n)$[59,60]. The bilayer form factor $F(q_z)$, which is in general a complex quantity, is real-valued in the case of centro-symmetry. The phase problem of crystallography, therefore, simplifies to the sign problem $F(q_z) = \pm|F(q_z)|$. and the phases, ν_n, can only take the values ± 1. The phases ν_n are needed to reconstruct the electron density profile from the scattering data following Equation (1). When the membrane form factor $F(q_z)$ is measured at several q_z values, a continuous function, $T(q_z)$, which is proportional to $F(q_z)$, can be fitted to the data[59–62]:

$$T(q_z) = \sum_n \sqrt{I_n q_n}\,\mathrm{sinc}\left(\frac{1}{2}d_z q_z - \pi n\right). \quad (2)$$

Once an analytical expression for $T(q_z)$ has been determined from fitting the experimental peak intensities, the phases ν_n can be assessed from $T(q_z)$.

In order to put ρ_z on an absolute scale, the electron densities were scaled to fulfil the condition $\rho(0)$=0.22 e/Å^3 (the electron density of a CH_3 group) in the centre of the bilayer, and $\rho(d_z/2)$=0.33 e/Å^3 (the electron density of water, ρ_W) outside the bilayers. All samples were well fit by the phase array [$\bar{1}$ $\bar{1}$ 1 $\bar{1}$ 1 $\bar{1}$ 1 $\bar{1}$ 1 $\bar{1}$]. Up to 11 pronounced Bragg peaks were observed resulting in a high spatial resolution.

The d_z-spacing between two neighbouring membranes in the stack was determined from the distance between the well developed Bragg reflections ($d_z = 2\pi/\Delta q_z$). The reflectivity peaks were well fit by Gaussian peak profiles. To assign the peaks to different phases, Bragg's law can be re-written as $\sin(\theta) = \lambda/(2d_z) \times n$. By plotting the sine of the Bragg angles versus the order of the different Bragg reflections, $\sin(\theta(n))$ vs. n, peaks which belong to the same d_z-spacing fall on a straight line through the origin, whose slope is proportional to $1/d_z$. Note that not all diffraction orders are necessarily observed for the different d_z-spacings as their scattering intensity depends on the form factor of the bilayers and oscillates between zero and maximum intensity as a function of q_z.

Sample	DMPC (mol%)	cholesterol (mol%)	ASA (mol%)	Unit Cell	Area per lipid (Å^2)	d_z^{lipid} (Å)	Area per cholesterol (Å^2)	d_z^{chol} (Å)
1	100	0	0	head groups: a_H=8.77 Å, b_H=9.31 Å, γ_H=90° lipid tails: a_T=4.97 Å, b_T=8.25 Å, γ_T=94.18°	40.84 ± 0.1	52.6 ± 0.1	–	–
2	80	20	0	a_T=5.03 Å,γ_H=120°	44 ± 1	50.1±0.1	-	-
3	70	30	0	a_T=5.12 Å,γ_H=120°	45.2 ± 2	50.5±0.1	-	-
4	60	40	0	lipid tails: a_T=4.48 Å, γ_T=120° chol monoclinic: a=10.70 Å, b=8.60 Å, γ=103.0°	34.8 ± 0.1	50.9 ± 0.1	44.83 ± 0.1	32.5±0.3
5	95	0	5	a_T=4.86 Å,γ_H=120°	41 ± 1	55.3	-	-
6	80	15	5	a_T=4.90 Å,γ_H=120°	41.6 ± 1	49.1	-	-
7	65	30	5	a_T=5.10 Å,γ_H=120°	45.2 ± 1.5	48.89	-	-
8	55	40	5	lipid tails: a_T=4.45 Å, γ_T=120° chol monoclinic: a=10.37 Å, b=8.4 Å, γ=103.0°	34.2 ± 0.5	43.8 ± 0.3	42.44 ± 0.1	34.3±0.1
9	90	0	10	a_T=4.86 Å,γ_H=120°	41 ± 1	53	-	-
10	75	15	10	a_T=4.91 Å,γ_H=120°	42 ± 1.5	51.55	-	-
11	60	30	10	a_T=5.06 Å,γ_H=120°	45.2±2	44.5	-	-
12	50	40	10	lipid tails: a_T=4.58 Å, γ_T=120° chol monoclinic: a=10.4 Å, b=8.27 Å, γ=103.0°	36.3 ± 0.1	44.4 ± 0.1	42.0 ± 0.1	34.4±1.7
13	62.5	30	7.5	a_T=5.15 Å,γ_H=120°	45.9 ± 1.5	50	-	-
14	57.5	30	12.5	a_T=5.18 Å,γ_H=120°	46.5 ± 1.5	50	-	-
15	52.5	40	7.5	lipid tails: a_T=4.62 Å, γ_T=120° chol monoclinic: a=10.64 Å, b=8.4 Å, γ=103.0°	37.0 ± 0.1	43.1 ± 0.1	43.5 ± 0.1	34.2±0.1
16	47.5	40	12.5	lipid tails: a_T=4.83 Å, γ_T=120°	40.5 ± 0.1	41.8 ± 0.5	-	34.11±0.1

TABLE 1. List of all the samples prepared for this study and their molecular composition. Unit cell dimensions, area per lipid and cholesterol molecules and the lamellar spacings for lipid and cholesterol bilayers (d_z^{lipid} and d_z^{chol}) are also given. See text for details.

3. RESULTS

Sixteen different samples were created containing varied amounts of DMPC, ASA and cholesterol. Samples with up to 12.5 mol% ASA and 40 mol% cholesterol were prepared, as listed in Table 1. Two-dimensional X-ray intensity maps were gathered for all samples, with select samples displayed in Figure 2.

Some qualitative conclusions can be drawn from the 2-dimensional maps. As shown in Figure 2 a), a number of Bragg peaks are scattered for pure DMPC along $q_{||}$, caused by long range order of lipid tails and lipid head groups in the plane of the membrane, as discussed for instance in[46,63,64]. However, as shown in Figure 2 b) at 30 mol% cholesterol, long range lateral order is suppressed and a single broad Bragg peak is observed along $q_{||}$, indicative of a disordered system with a range of nearest-neighbour distances due to the inclusion of cholesterol[30,46,65].

At 40 mol% cholesterol in Figure 2 c), additional Bragg peaks were observed along the out-of-plane and in-plane axes, related to the formation of immiscible cholesterol plaques, i.e., cholesterol bilayers coexisting with the lamellar membrane structure, as reported previously by Barrett *et al*[39]. The intensity of these peaks was found to increase in the presence of 5 mol% ASA in Figure 2 d). Addition of 10 mol% ASA in part e) led to a decrease of the intensity of the cholesterol Bragg peaks indicating a shrinking fraction of cholesterol plaques.

For a quantitative analysis of the diffracted intensity, the 2-dimensional data were cut along the out-of-plane and in-plane axes. As in-plane features are usually orders of magnitude weaker than the pronounced out-of-plane reflections, slices 0.03 Å$< q_z <$ 0.3 Å were integrated to enhance the data quality.

3.1. *Out-Of-Plane Structure and Electron Densities*

The position of ASA and cholesterol molecules along the membrane normal, and the bilayer spacing, d_z, were determined from the out-of-plane scans. Reflectivities for samples 1,3 and 11 are shown in Figures 3 a)-c). The peaks are pronounced and equally spaced, indicative of a well-organized lamellar membrane structure. The assembled electron density profiles are shown in Figures 3 d) and e), along with cartoons suggesting approximate positions for the molecules along the membrane normal.

Figure 3 d) displays the electron density profiles for a pure DMPC membrane as well as for a membrane prepared with 30 mol% cholesterol. The profile for pure DMPC corresponds to a DMPC molecule in the well ordered gel state with both chains in all-trans configuration, as has been reported previously by the Nagle group[46,58]. The electron rich phosphorous group in the head group region can easily be identified by the peak in the electron density at ∼22 Å. ρ_z monotonically decreases towards the bilayer centre at $z = 0$ to $\rho(0)$=0.22 e$^-$Å^{-3}, the electron density of a CH_3 group[46,66].

The electron density in the central region of the lipid

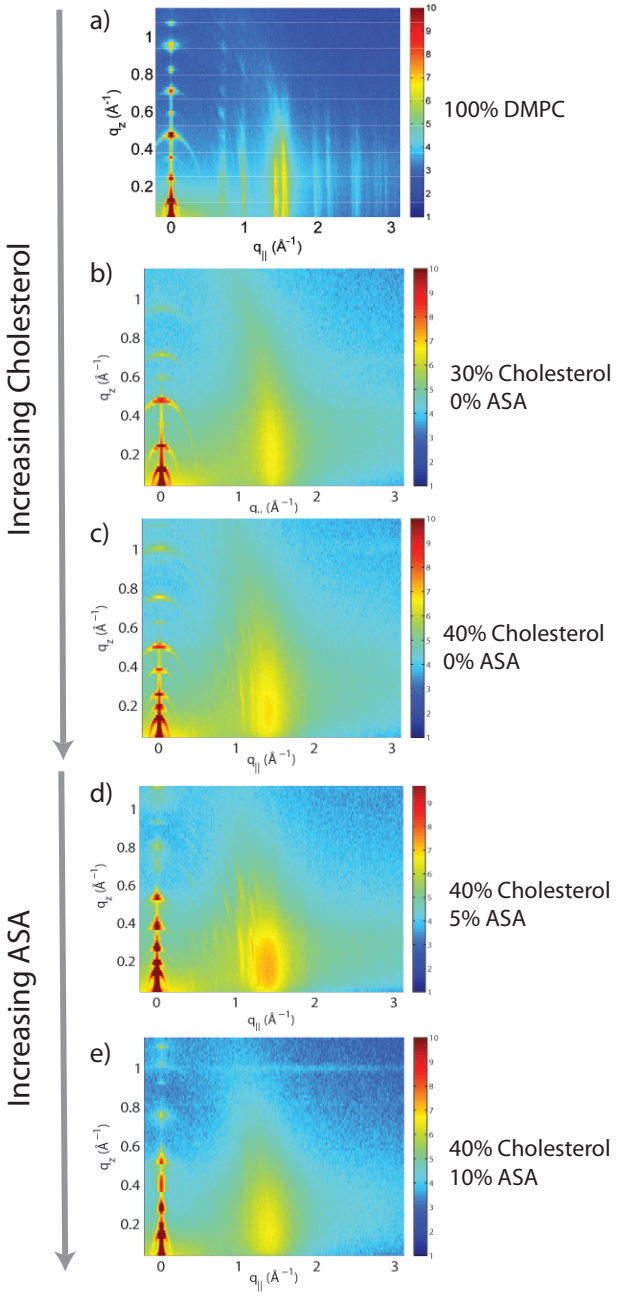

FIG. 2. Two-dimensional X-ray intensity maps of samples 1,3,4,8,12: a) 100 mol% DMPC, b) 30 mol% Cholesterol, c)40 mol% Cholesterol, d)5 mol% ASA + 40 mol% Cholesterol, e) 10 mol% ASA + 40 mol% Cholesterol in DMPC.

tails was found to increase in the presence of cholesterol, as shown in Figure 3 d). As depicted in the Figure, a cholesterol molecule can be fitted at z values of 2 Å$< z <$19 Å, with the hydrophilic, electron-rich oxygen groups at a z position of ∼18 Å. This orientation is compatible with the well known umbrella model[34,36] and "protects" the hydrophobic part of the cholesterol molecule from the aqueous environment, as reported previously for cholesterol in saturated phospholipid bilayers made of DMPC and DPPC[8,39,67]. The umbrella model suggests[68,69] that cholesterol molecules associate strongly with ordered hydrocarbon chains (usually ones that are fully saturated) in such a manner that they are shielded from contact with the aqueous environment by the lipid head group. The electron density in Figure 3 d) also demonstrates that the cholesterol molecules are not lying flat between the two leaflets, as was reported recently for highly unsaturated lipid bilayers[28,37].

Figure 3 e) shows the profile of the 30 mol% cholesterol sample, along with a sample prepared with 30 mol% and 10 mol% ASA. This mixture was found to still form homogenous, multi lamellar structures. The sample prepared with ASA shows an overall reduced electron density because more electron rich lipid molecules were replaced by smaller ASA molecules. A pronounced loss of electron density is observed near the head group region at z values of ∼21 Å, as was shown previously by *Barrett et al.*[46] As depicted in the Figure, an ASA molecule can be fitted at z values of 16 Å$< z <$21 Å, with the hydrophilic, electron-richer oxygen groups at a z position of ∼21 Å, pointing towards the hydration water. This orientation "protects" the hydrophobic part of the ASA molecule from the aqueous environment. Figure 3 e) demonstrates that ASA and cholesterol molecules coexist in lipid membranes, in particular at high concentrations of cholesterol and ASA. While the cholesterol molecules take an upright position in the hydrophobic membrane core parallel to the lipid acyl chains, the ASA molecules reside preferably in the lipid head group region.

The lamellar spacing, the distance between two bilayers in the membrane stack, was determined from the position of the out-of-plane peaks. When the data is presented as $\sin(\theta)$, the Bragg angle of the lamellar peaks versus the order of the reflection, n, the slope of the fitted line is a function of the lamellar spacing, d_z. The corresponding data for samples 4,8,12,15 and 16 for DMPC/40 mol% and ASA concentrations from 0 mol% to 12.5 mol% are shown in Figure 4.

As was reported previously, two lamellar spacings are observed at 40 mol% cholesterol due to the presence of immiscible cholesterol plaques. As described by Barrett *et al.*[39], these extra peaks are due to a coexisting, immiscible cholesterol bilayer within the larger lipid structure[39]. The data in Figure 4 were all well fit by two lines through the origin corresponding to two distinct d_z-spacings. Three lines could be assigned to the 12.5 mol% sample in Figure 4 e), as will be discussed below. The different d_z-spacing, labeled as d_z, d'_z and d''_z, were determined from the slopes and are given in the Figures as well as in Table 1.

3.2. Lateral Membrane Structure

Molecular order of lipids, cholesterol, and ASA molecules in the plane of the membrane was determined from scattering patterns observed along $q_{||}$, as shown

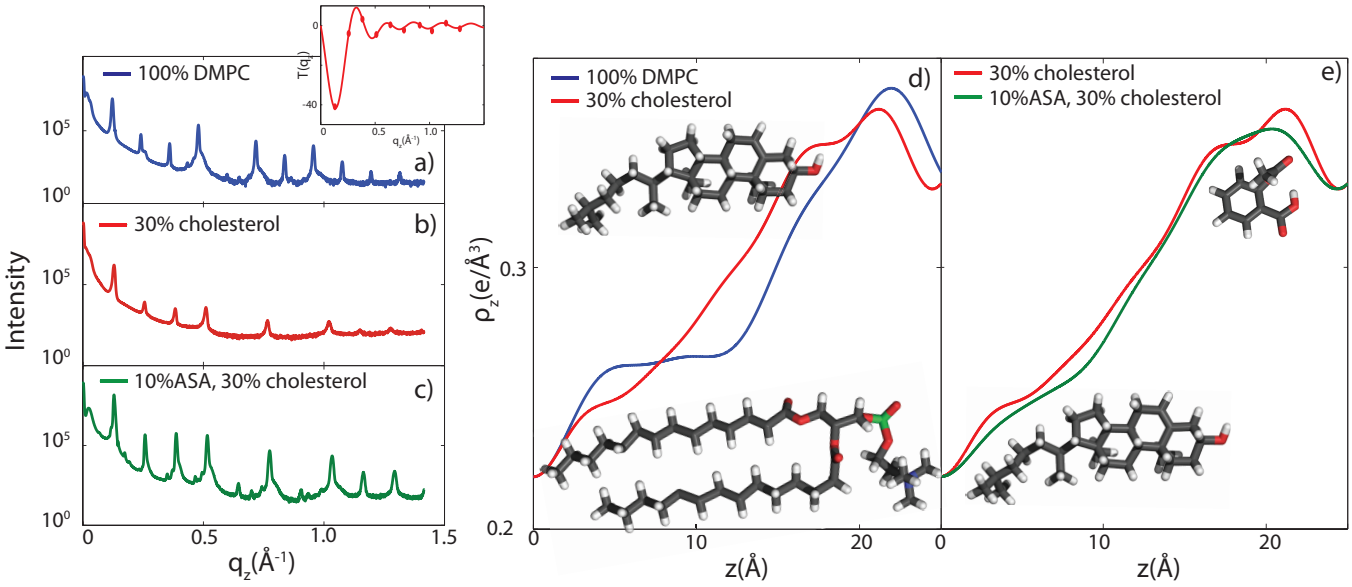

FIG. 3. Reflectivities and corresponding electron density profiles. a) Reflectivity for a sample with 100 mol% DMPC b) 30 mol% cholesterol c) 30 mol% cholesterol and 10 mol% ASA. $T(q_z)$ is shown exemplarily for 30 mol% cholesterol as inset to part a). d) Electron density profiles for samples with 100% DMPC (blue) and 70 mol% DMPC with 30 mol% cholesterol (red). e) Electron profiles for a samples with 30 mol% cholesterol (red) and 30 mol% cholesterol with 10 mol% ASA (green). Approximate positions of the molecules are shown.

in Figure 5. As discussed in[46,63,64], Bragg peaks of a pure DMPC sample are indexed by an orthorhombic head group lattice, while the tails form a monoclinic unit cell.

Only one peak was observed for samples from 0 mol% cholesterol up to 30 mol% cholesterol, and from 0 mol% ASA up to 12.5 mol% ASA (for samples with 30 mol% cholesterol or less). The presence of small amounts of ASA or cholesterol inhibits long range order, as evidenced by the absence of Bragg peaks as described previously[39,46]. This is likely due to a stochastic distribution of ASA and cholesterol molecules in the plane of the membrane. The lipid tails form a densely packed structure with hexagonal symmetry[35]. In the absence of fluctuations, the area per lipid molecule can be determined from the position of the Bragg peak scattered in plane at a $q_{||}$ position of q_T. The area per lipid is calculated using $A_L = 16\pi^2/(\sqrt{3}q_T^2)$. The distance between two acyl tails is determined to be $a_T = 4\pi/(\sqrt{3}q_T)$, with the area per lipid simplifies of $A_L = \sqrt{3}a_T^2$. The area per lipid for all samples are listed in Table 1.

Additional in-plane Bragg peaks were observed at 40 mol% cholesterol and were assigned to the structure of cholesterol molecules in coexisting cholesterol bilayer plaques. A cartoon depicting one of these plaques is shown in Figure 5 a). In plane intensity from the sample prepared with 40 mol% cholesterol is shown in figure 5 b), plotted as function of the in-plane scattering angle $2\theta_\chi$. There is a broad Bragg peak at $\approx 20°$, and a number of additional, narrow peaks. The structure of the cholesterol bilayers could be determined from the additional narrow peaks. As detailed in[39], for a sample with 40 mol% cholesterol the additional in-plane Bragg peaks can be assigned to a monoclinic unit cell, with parameters a=10.7 Å, b=8.6 Å, $\alpha = \beta = 90°$ and $\gamma = 103°$. Based on this model, the additional Bragg peaks are labelled with their corresponding Miller indices in Figure 5.

In plane peaks from Samples containing 40 mol% cholesterol and between 5 mol% and 10 mol% ASA are depicted in Figures 5 c)-e). These samples also show additional, narrow Bragg peaks along with the broad lipid tail peak. Additional Bragg peaks are located at nearly identical positions along $2\theta_\chi$, suggesting that the structure of the cholesterol plaques is unchanged by the addition of ASA. However, the intensity of these peaks was found to drastically decrease with increasing ASA.

4. DISCUSSION

4.1. *Effect of Aspirin*

The impact of Aspirin and its metabolites on the body are usually studied with regards to their effects on the cyclo-oxygenase (COX) pathway. The COX pathway contributes to platelet aggregation. The inhibition of COX-1 and COX-2 by higher dose Aspirin is understood to cause analgesic and anti-inflammatory effects, whereas lower doses, enough to inhibit COX-1 activity, are sufficient for anti-platelet activity[70,71]. The anti platelet activity leads to reduced blood clot formation and hence reduced blockage of arteries and increased blood flow. However, there is growing evidence for the

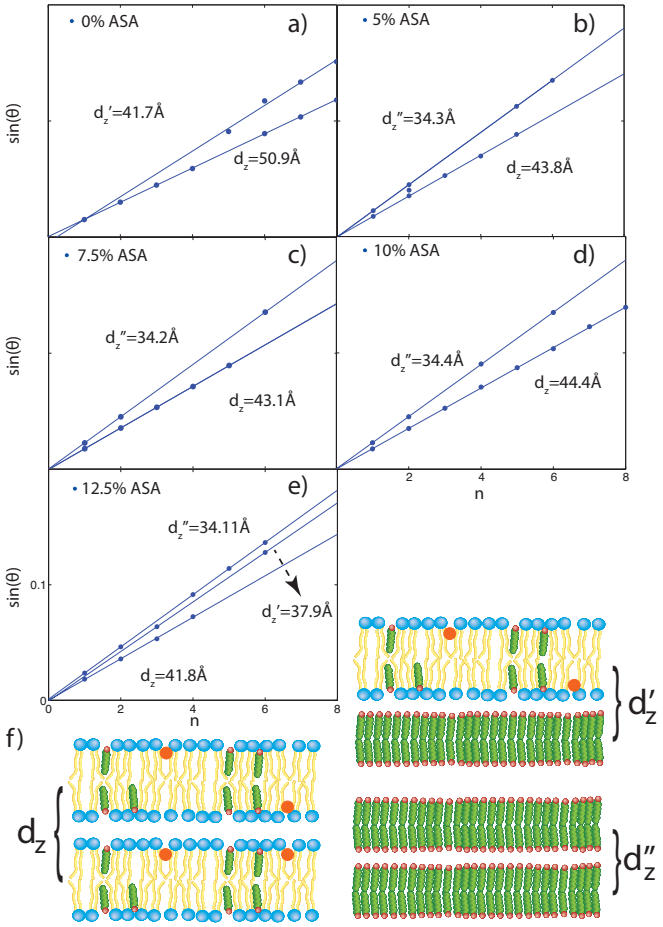

FIG. 4. Position of out-of-plane peaks, $\sin(\theta)$ vs Bragg order n for a) 40 mol% cholesterol b) 40 mol% cholesterol and 5 mol% ASA c) 40 mol% cholesterol and 7.5 mol% ASA d) 40 mol% cholesterol and 10 mol% ASA e) 40 mol% cholesterol and 12.5 mol% ASA. The slope of the line is proportional to the lamellar spacing, d_z. The corresponding bilayer distances are indicated next to the slopes. Cartoons depict two adjacent lipid bilayers, a lipid bilayer adjacent to a cholesterol bilayer and two stacked cholesterol bilayers.

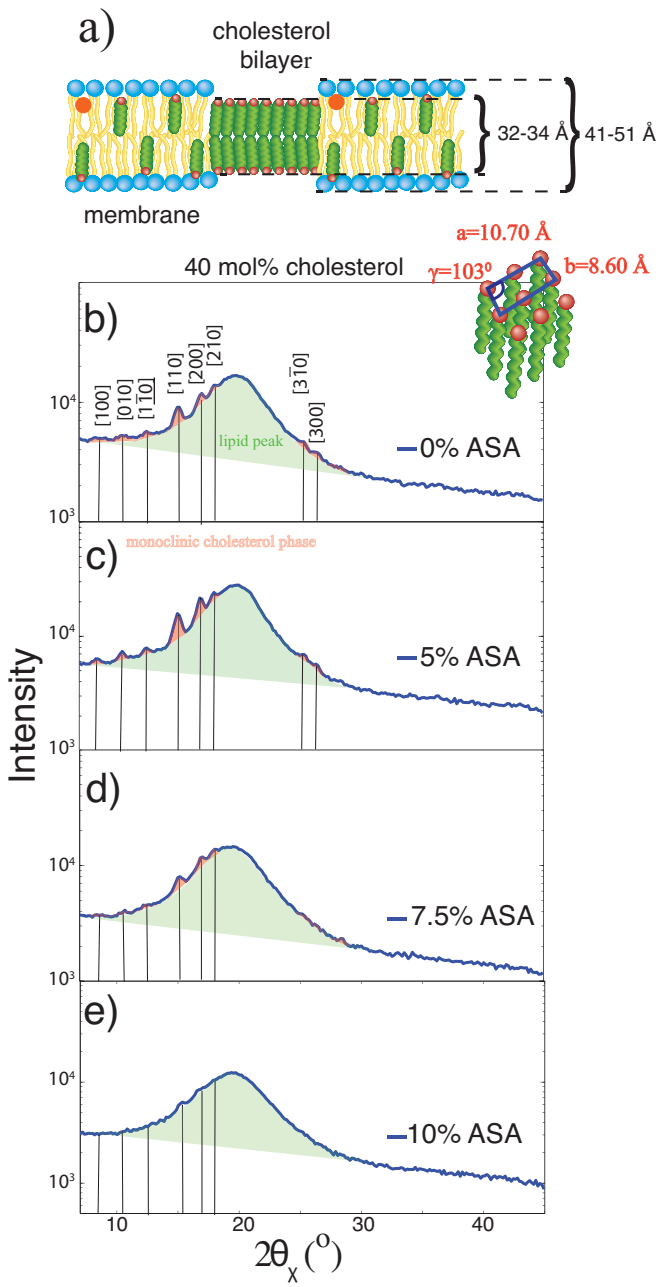

FIG. 5. a) Cartoon depicting a cholesterol bilayer coexisting with a DMPC bilayer. b)-e): In-plane scans for samples with 0 mol% ASA 5 mol% ASA, 7.5 mol% ASA, and 10 mol% ASA all with 40 mol% cholesterol. The vertical lines indicate the positions of the monoclinic Bragg peaks associated with cholesterol molecules in the cholesterol bilayer, with the appropriate Miller indices indicated in b).

influence of Aspirin beyond the COX pathway, and for an influence of Aspirin and other NSAID's on the lipid membrane[72–74]. Aspirin has been shown to have a high affinity for phospholipids[47], and to perturb lipid bilayers in a concentration dependent manner[75]. Suwalsky *et al.*[75] found that ASA strongly perturbed model membranes made of DMPC and DMPE, predominantly found in the outer and inner monolayers of the human erythrocyte membrane and observed that aspirin affects the human erythrocyte shape. In addition, non-steroidal anti-inflammatory drugs such as Aspirin and Ibuprofen have been shown to increase membrane fluidity and the incidence of pores, decrease the hydrophobic surface barrier, leading to diffusion of acid and cellular injury.[47,49,76].

There is also growing evidence for the effect of lipid organization on platelet function. Increased platelet aggregation has been associated with decreased platelet membrane fludity[77–79], and platelet aggregation has been associated with lipid rafts. In addition, β-carbolines were found to inhibit platelet activity by modifying platelet membrane fluidity[80]. Our results add to the growing evidence for Aspirin's effect on the lipid membrane, and highlight the ability of Aspirin to re-organize the membrane.

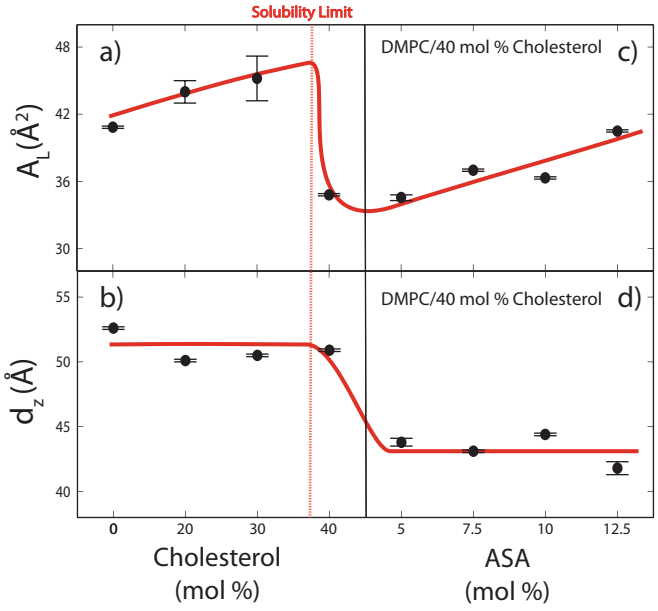

FIG. 6. a) Area per lipid, A_L, and b) d_z-spacing as function of increasing cholesterol concentration in the DMPC bilayers. The red line indicates the solubility limit of cholesterol in model DMPC membranes of ∼37.5 mol%[39]. Parts c) and d) show the effect of addition of ASA to a DMPC/40 mol% cholesterol membrane, where cholesterol plaques formed. Addition of ASA leads to an increase in lipid area, while the lamellar spacing did not change within the resolution of the present experiment.

4.2. The Interaction of Aspirin with Membranes

Membranes containing ASA were previously studied using X-ray diffraction[46,75,81]. While cholesterol is known to reside in the hydrophobic membrane core and to align parallel to the saturated lipid tails (see, e.g.,[8,67]), in agrement with the umbrella model, ASA is located among the head groups of the lipid molecules. The formation of cholesterol plaques in model membranes at high cholesterol levels was reported recently[39] and a model for initiation of atherosclerosis from cholesterol crystal nuclei formed at the cell membrane interface has been proposed[82].

As reviewed recently by Pereira-Leite, Nunes and Reis[74], studies are typically performed with NSAID concentration in the range of μM, which is close to the plasma concentration of NSAIDs, but also in the range of mM[75].

K_p values of up to K_p ∼3200 were reported for different NSAIDs in DMPC suspensions[83] (see the Appendix for a conversion between K_p and molar concentrations). These coefficients correspond to molar concentrations on the order of ∼10 mol%, i.e., concentrations of 1 ASA molecule per about 10 lipid molecules in the bilayers. The ASA concentrations in Table 1 are certainly elevated as compared to plasma concentrations of less than 1 mol%, however comparable to ASA concentrations typically used in the literature.We note that the measurements in this study were conducted in synthetic model membranes at very high ASA concentrations. Despite the fact that our findings are very conclusive, we can, at this point, not comment on the physiological relevance.

The formation of cholesterol plaques depends on the solubility limit of cholesterol in membranes, which is strongly dependent on the lipid composition of the corresponding bilayers. The solubility limits for model membranes made of saturated DMPC and DPPC were recently reported to be 40 mol%[39] and 37.5 mol%[35] cholesterol, respectively. Plaques were observed already at physiological concentrations of 30 mol% cholesterol in anionic lipid model membranes consisting of 97 mol% DMPC/3 mol% DMPS[84] such that the observed effect of ASA should be even more pronounced in charged membranes. We can, at this point, not comment on the relevance of the effect in unsaturated or poly-unsaturated lipid membranes, which more closely mimic the composition of plasma membranes, as the corresponding solubility limits have not yet been reported in the literature. However, dimyristoylphosphatidylcholine represents phospholipid classes in the human erythrocyte membranes[75].

4.3. Structure of the Membranes Containing Cholesterol and ASA

The lamellar spacings of the membrane complexes together with the areas per membrane molecule were determined from the analysis of the out-of-plane and in-plane diffraction data, as listed in Table 1. The corresponding data are plotted in Figure 6. The area per lipid was found to increase from ∼41 Å^2 to ∼45 Å^2 with increasing cholesterol content until immiscible cholesterol plaques formed at ∼40 mol% cholesterol, in agreement with Barrett *et al.*[39]. We then studied the effect of ASA on the cholesterol plaques at a cholesterol concentration of 40 mol%, close to the solubility limit of cholesterol in DMPC model membranes. The area per lipid was found to increase with the addition of ASA. Up to 12.5 mol% ASA were added to the DMPC/40 mol% cholesterol membranes. The lamellar d_z-spacing was approximately constant with increasing cholesterol and dropped from ∼52 Å to ∼43 Å when ASA was added. Increasing the amount of ASA did not change the d_z-spacing within the resolution of this experiment. The increase in the lipid area at constant d_z in Figure 6 is indicative of an increase in lipid volume by ∼20%, from ∼1400 Å^3 to 1700 Å^3. This increase in volume is indicative of an increase in fluidity of the bilayers in the presence of ASA.

Given the high lipid:cholesterol ratio of about 1:1, where precipitation was observed, different scenarios can be envisioned. A given membrane in the stack can be adjacent to 1) another membrane, 2) a cholesterol bilayer or 3) two cholesterol plaques stack, as pictured in Figure 4 f).

Three d_z-spacings, d_z, d'_z and d''_z were observed in the data in Figure 4 e) for the highest concentration of ASA of 12.5 mol%. The larger d_z-spacing agrees well with the distance between two membranes in the stack. This d_z-spacing is equivalent to the thickness of a bilayer including the water layer that separates neighbouring bilayers in the stack. The second, smaller d_z (d'_z in Figure 4 f) and in Table 1) spacing was indicative of a coexisting, smaller repeat distance. d'_z-spacing involved a bilayer and an adjacent cholesterol bilayer such that $d'_z = \frac{1}{2}d_{\mathrm{lipid}} + \frac{1}{2}d_{\mathrm{chol}}$, which gives $d_{\mathrm{chol}} = 2 \times d'_z - d_{\mathrm{bilayer}}$. The corresponding values for d_{chol} vary between 32.5 Å and 34.2 Å and are listed in Table 1. Given the length of a cholesterol molecule of ∼17 Å, these values are in excellent agreement with a cholesterol bilayer, where the cholesterol molecules are oriented along the perpendicular z direction, as sketched in Figure 5 a). The smallest lamellar spacing, d''_z, was directly equivalent to the thickness of a cholesterol bilayer, d_{chol}, as depicted in Figure 4 f). We note that d_{chol} determined from d'_z and d''_z, are in excellent agreement, which strongly supports the model in Figure 4 f).

Additional in-plane Bragg reflections were observed in Figure 5 a) when the immiscible cholesterol plaques formed. As reported previously[39–42,45], the cholesterol molecules in the cholesterol bilayer organize laterally in a monoclinic unit cell at this concentration.

4.4. Effect of ASA on Cholesterol Plaques

The intensity of the corresponding Bragg peaks in Figure 5 is directly proportional to the volume fraction of the cholesterol molecules participating in plaques. The corresponding area of the monoclinic peaks was determined by fitting the peaks to Lorentzian peak profiles and normalized to the total intensity scattered into monoclinic and lipid peaks. The normalized area is plotted in Figure 7. The fraction of cholesterol plaques initially increased when 5 mol% ASA molecules were included. The ratio between lipid and cholesterol molecules increased from 40 mol% to ∼42 mol% as lipid and cholesterol molecules made only 95% of the bilayers. However, despite the fact that the ratio between lipid and cholesterol kept decreasing when increasing the amount of ASA molecules, the volume fraction of cholesterol plaques drastically decreased until no peaks could be detected at an ASA concentration of 12.5 mol%.

From the data in Figures 6 and 7, the inclusion of ASA molecules in membranes containing cholesterol led to a re-fluidification of the bilayers and to a decomposition of immiscible cholesterol plaques. We note that signs of cholesterol plaques were still detected in the out-of-plane scans in Figure 4 e) while no in-plane signals could be detected within the resolution of this experiment. The lamellar Bragg peaks are usually orders of magnitude stronger in highly-aligned stacked membrane systems than the in-plane scattering. We can, therefore, not exclude that small cholesterol plaques were still present at 40 mol% cholesterol and 12.5 mol% ASA. We note that the cholesterol:lipid ratio was increased to 46 mol% in this sample. However the volume fraction of plaques was drastically reduced as compared to a DMPC/40 mol% cholesterol system.

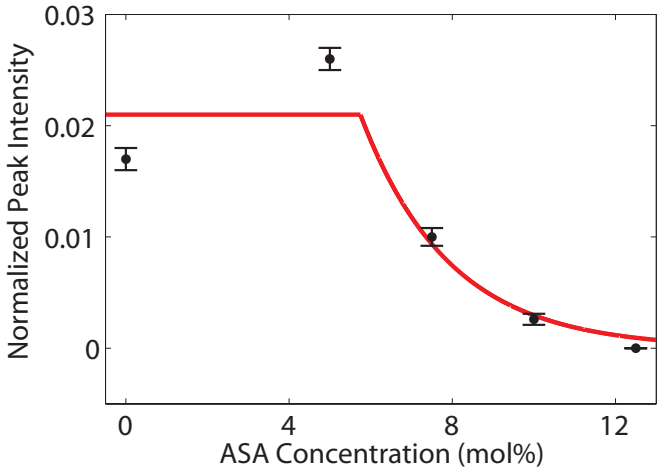

FIG. 7. Normalized integrated area of the monoclinic cholesterol Bragg peaks as function of ASA concentration. The volume fraction of the immiscible cholesterol plaques shows an initial increase before decreasing at higher ASA concentrations. No immiscible domains were observed in the in-plane scans at 12.5 mol% ASA.

5. CONCLUSION

The molecular out-of-plane and in-plane structures of highly oriented, solid supported membranes containing up to 12.5 mol% ASA and 40 mol% cholesterol were studied using high-resolution X-ray diffraction. ASA and cholesterol were found to coexist within saturated lipid membranes made from DMPC, even at high levels of cholesterol and ASA of up to 40 mol% cholesterol and 12.5 mol% ASA. The cholesterol molecules partitioned in the hydrophobic membrane aligning parallel to the lipid acyl chains, in agreement with the umbrella model, while the ASA molecules were found to reside in the lipid head group region.

High cholesterol concentrations above 40 mol% led to the formation of immiscible cholesterol plaques, in agreement with previous studies. Increasing the amount of ASA in the membranes resulted in a a significant increase in fluidity of the bilayers and dissolved the cholesterol plaques. These results add to the growing evidence for Aspirin's effect on the lipid membrane. Our results present experimental evidence for an interaction between cholesterol and ASA on the level of the cell membrane. Further investigations will clarify if the observed effect is the result of a direct ASA-cholesterol interaction or a general effect of the increased fluidity of the membranes

due to the presence of ASA.

ACKNOWLEDGMENTS

This research was funded by the Natural Sciences and Engineering Research Council (NSERC) of Canada, the National Research Council (NRC), the Canada Foundation for Innovation (CFI), and the Ontario Ministry of Economic Development and Innovation. H.D. is the recipients of NSERC Undergraduate Research Awards (USRA). M.C.R. is the recipient of an Early Researcher Award from the Province of Ontario.

Appendix: Calculation of Partitioning Coefficients

The molar coefficient of ASA partitioning into lipid bilayers, K_p, is defined as $K_p = X^{ASA}_{lipid}/X^{ASA}_{water}$, where X^{ASA}_{lipid} and X^{ASA}_{water} are the mole fractions of ASA in lipid and water phases, respectively. K_p can also be expressed using molar ratios $K_p = \frac{677.933}{18.015} \times molar\ ratio^{ASA}_{lipid}/molar\ ratio^{ASA}_{water}$, with M_{lipid}=677.933 g/mol the molar weight of a DMPC molecule and M_{water}=18.015 g/mol the molar mass of water.

* rheinstadter@mcmaster.ca

[1] Singer SJ, Nicolson GL (1972) The fluid mosaic model of the structure of cell membranes. Science 175: 720–731.
[2] Mouritsen OG (2005) Life-as a matter of fat: the emerging science of lipidomics. Springer.
[3] Rheinstädter MC, Mouritsen OG (2013) Small-scale structure in fluid cholesterol-lipid bilayers. Curr Opin Colloid Interface Sci 18: 440-447.
[4] Vereb G, Szöllősi J, Matko J, Nagy P, Farkas T, et al. (2003) Dynamic, yet structured: the cell membrane three decades after the singer–nicolson model. Proc Natl Acad Sci USA 100: 8053–8058.
[5] Bloch KE (1983) Sterol, structure and membrane function. Crit Rev Biochem Mol Biol 14: 47–92.
[6] Yeagle PL (1985) Lanosterol and cholesterol have different effects on phospholipid acyl chain ordering. BBA-BIOMEMBRANES 815: 33–36.
[7] Vist MR, Davis JH (1990) Phase equilibria of cholesterol/dipalmitoylphosphatidylcholine mixtures: deuterium nuclear magnetic resonance and differential scanning calorimetry. Biochemistry 29: 451–464.
[8] Armstrong CL, Barrett MA, Hiess A, Salditt T, Katsaras J, et al. (2012) Effect of cholesterol on the lateral nanoscale dynamics of fluid membranes. Eur Biophys J 41: 901–913.
[9] Armstrong CL, Häußler W, Seydel T, Katsaras J, Rheinstädter MC (2014) Nanosecond lipid dynamics in membranes containing cholesterol. Soft Matter 10: 2600-2611.
[10] Simons K, Ikonen E (1997) Functional rafts in cell membranes. Nature 387: 569572.
[11] Simons K, Ikonen E (2000) How cells handle cholesterol. Science 290: 1721-1726.
[12] Engelman DM (2005) Membranes are more mosaic than fluid. Nature 438: 578-580.
[13] Niemelä PS, Ollila S, Hyvnen MT, Karttunen M, Vattulainen I (2007) Assessing the nature of lipid raft membranes. PLoS Comput Biol 3: e34.
[14] Pike LJ (2009) The challenge of lipid rafts. J Lipid Res 50: S323–S328.
[15] Lingwood D, Simons K (2009) Lipid rafts as a membrane-organizing principle. Science 327: 4650.
[16] Eggeling C, Ringemann C, Medda R, Schwarzmann G, Sandhoff K, et al. (2009) Direc observation of the nanoscale dynamics of membrane lipids in a living cell. Nature 457: 1159-1162.
[17] van der Goot FG, Harder T (2001) Raft membrane domains: from a liquid-ordered membrane phase to a site of pathogen attack. Semin Immunol 13: 89 - 97.
[18] Lenne PF, Nicolas A (2009) Physics puzzles on membrane domains posed by cell biology. Soft Matter 5: 2841–2848.
[19] Apajalahti T, Niemelä P, Govindan PN, Miettinen MS, Salonen E, et al. (2009) Concerted diffusion of lipids in raft-like membranes. Faraday Discuss : 2010.
[20] Hall A, Róg T, Karttunen M, Vattulainen I (2010) Role of glycolipids in lipid rafts: A view through atomistic molecular dynamics simulations with galactosylceramide. J Phys Chem B 114: 7797-7807.
[21] Simons K, Gerl MJ (2010) Revitalizing membrane rafts: new tools and insights. Nat Rev Mol Cell Biol 11: 688-699.
[22] Hansson L, Zanchetti A, Carruthers SG, Dahlöf B, Elmfeldt D, et al. (1998) Effects of intensive blood-pressure lowering and low-dose aspirin in patients with hypertension: principal results of the hypertension optimal treatment (hot) randomised trial. The Lancet 351: 1755–1762.
[23] Weisman SM, Graham DY (2002) Evaluation of the benefits and risks of low-dose aspirin in the secondary prevention of cardiovascular and cerebrovascular events. Arch Intern Med 162: 2197.
[24] Ridker PM, Manson JE, Gaziano JM, Buring JE, Hennekens CH (1991) Low-dose aspirin therapy for chronic stable anginaa randomized, placebo-controlled clinical trial. Ann Intern Med 114: 835–839.
[25] McIntosh TJ (1978) The effect of cholesterol on the structure of phosphatidylcholine bilayers. Biochimica et Biophysica Acta (BBA)-Biomembranes 513: 43–58.
[26] Vance DE, Van den Bosch H (2000) Cholesterol in the year 2000. BBA-MOL CELL BIOL L 1529: 1–8.
[27] Pan J, Mills TT, Tristram-Nagle S, Nagle JF (2008) Cholesterol perturbs lipid bilayers nonuniversally. Phys Rev Lett 100: 198103.
[28] Kučerka N, Marquardt D, Harroun T, Nieh MP, Wassall S, et al. (2009) The functional significance of lipid diversity: Orientation of cholesterol in bilayers is determined by lipid species. J Am Chem Soc 131: 16358.
[29] Pan J, Tristram-Nagle S, Nagle JF (2009) Effect of cholesterol on structural and mechanical properties of membranes depends on lipid chain saturation. Phys Rev E 80: 021931.

[30] Mills T, Huang J, Feigenson G, Nagle J (2009) Effects of cholesterol and unsaturated dopc lipid on chain packing of saturated gel-phase dppc bilayers. Gen Physiol Biophys 28: 126-139.

[31] Pabst G, Kučerka N, Nieh MP, Rheinstädter M, Katsaras J (2010) Applications of neutron and x-ray scattering to the study of biologically relevant model membranes. Chem Phys Lipids 163: 460 - 479.

[32] Mouritsen OG (2010) The liquid-ordered state comes of age. BBA-BIOMEMBRANES 1798: 1286–1288.

[33] Marsh D (2010) Liquid-ordered phases induced by cholesterol: A compendium of binary phase diagrams. Biochimica et Biophysica Acta (BBA) - Biomembranes 1798: 688 - 699.

[34] Dai J, Alwarawrah M, Huang J (2010) Instability of cholesterol clusters in lipid bilayers and the cholesterol?s umbrella effect. J Phys Chem B 114: 840-848.

[35] Armstrong CL, Marquardt D, Dies H, Kučerka N, Yamani Z, et al. (2013) The observation of highly ordered domains in membranes with cholesterol. PloS one 8: e66162.

[36] Huang J, Feigenson GW (1999) A microscopic interaction model of maximum solubility of cholesterol in lipid bilayers. Biophys J 76: 2142-2157.

[37] Kučerka N, Marquardt D, Harroun T, Nieh MP, Wassall S, et al. (2010) Cholesterol in bilayers with pufa chains: Doping with dmpc or popc results in sterol reorientation and membrane-domain formation. Biochemistry (Mosc) 49: 7485.

[38] Meinhardt S, Vink RLC, Schmid F (2013) Monolayer curvature stabilizes nanoscale raft domains in mixed lipid bilayers. Proc Natl Acad Sci USA 110: 4476-4481.

[39] Barrett M, Zheng S, Toppozini L, Alsop R, Dies H, et al. (2013) Solubility of cholesterol in lipid membranes and the formation of immiscible cholesterol plaques at high cholesterol concentrations. Soft Matter 9: 9342 - 9351.

[40] Rapaport H, Kuzmenko I, Lafont S, Kjaer K, Howes PB, et al. (2001) Cholesterol monohydrate nucleation in ultrathin films on water. Biophys J 81: 2729 - 2736.

[41] Solomonov I, Weygand MJ, Kjaer K, Rapaport H, Leiserowitz L (2005) Trapping crystal nucleation of cholesterol monohydrate: Relevance to pathological crystallization. Biophys J 88: 1809 - 1817.

[42] Solomonov I, Daillant J, Fragneto G, Kjaer K, Micha J, et al. (2009) Hydrated cholesterol: Phospholipid domains probed by synchrotron radiation. Eur Phys J A 30: 215-221.

[43] Ziblat R, Leiserowitz L, Addadi L (2010) Crystalline domain structure and cholesterol crystal nucleation in single hydrated dppc:cholesterol:popc bilayers. J Am Chem Soc 132: 9920-9927.

[44] Ziblat R, Leiserowitz L, Addadi L (2011) Crystalline lipid domains: Characterization by x-ray diffraction and their relation to biology. Angew Chem Int Ed 50: 3620–3629.

[45] Ziblat R, Fargion I, Leiserowitz L, Addadi L (2012) Spontaneous formation of two-dimensional and three-dimensional cholesterol crystals in single hydrated lipid bilayers. Biophys J 103: 255 - 264.

[46] Barrett M, Zheng S, Roshankar G, Alsop R, Belanger R, et al. (2012) Interaction of aspirin (acetylsalicylic acid) with lipid membranes. PLoS ONE 7: e34357.

[47] Lichtenberger LM, Zhou Y, Jayaraman V, Doyen JR, O'Neil RG, et al. (2012) Insight into nsaid-induced membrane alterations, pathogenesis and therapeutics: characterization of interaction of nsaids with phosphatidylcholine. BBA-MOL CELL BIOL L 1821: 994–1002.

[48] Zhou Y, Raphael RM (2005) Effect of salicylate on the elasticity, bending stiffness, and strength of sopc membranes. Biophys J 89: 1789–1801.

[49] Lichtenberger LM, Zhou Y, Dial EJ, Raphael RM (2006) Nsaid injury to the gastrointestinal tract: evidence that nsaids interact with phospholipids to weaken the hydrophobic surface barrier and induce the formation of unstable pores in membranes. J Pharm Pharmacol 58: 1421–1428.

[50] Vandenberg ET, Bertilsson L, Liedberg B, Uvdal K, Erlandsson R, et al. (1991) Structure of 3-aminopropyl triethoxy silane on silicon oxide. J Colloid Interface Sci 147: 103 - 118.

[51] Meyer HW, Semmler K, Rettig W, Pohle W, Ulrich AS, et al. (2000) Hydration of DMPC and DPPC at 4oc produces a novel subgel phase with convex-concave bilayer curvatures. Chem Phys Lip 105: 149-166.

[52] Nomura K, Lintuluoto M, Morigaki K (2011) Hydration and temperature dependence of 13c and 1h nmr spectra of the dmpc phospholipid membrane and complete resonance assignment of its crystalline state. J Phys Chem B 115: 14991–15001.

[53] de Meyer FJM, Benjamini A, Rodgers JM, Misteli Y, Smit B (2010) Molecular simulation of the dmpc-cholesterol phase diagram. J Phys Chem B 114: 10451-10461.

[54] Fragneto G, Rheinstädter M (2007) Structural and dynamical studies from bio-mimetic systems: an overview. C R Phys 8: 865-883.

[55] Rheinstädter MC, Seydel T, Demmel F, Salditt T (2005) Molecular motions in lipid bilayers studied by the neutron backscattering technique. Phys Rev E 71: 061908.

[56] Weik M, Lehnert U, Zaccai G (2005) Liquid-like water confined in stacks of biological membranes at 200 K and its relation to protein dynamics. Biophys J 89: 3639-3646.

[57] Hristova K, White SH (1998) Determination of the hydrocarbon core structure of fluid dioleoylphosphocholine (dopc) bilayers by x-ray diffraction using specific bromination of the double-bonds: Effect of hydration. Biophysical Journal 74: 2419 - 2433.

[58] Tristram-Nagle S, Liu Y, Legleiter J, Nagle JF (2002) Structure of gel phase dmpc determined by x-ray diffraction. Biophys J 83: 3324-3335.

[59] Nagle JF, Wiener MC (1989) Relations for lipid bilayers. Biophys J 55: 309-313.

[60] Nagle J, Zhang R, Tristram-Nagle S, Sun W, Petrache H, et al. (1996) X-ray structure determination of fully hydrated lα phase dipalmitoylphosphatidylcholine bilayers. Biophys J 70: 1419-1431.

[61] King GI, Worthington CR (1971) Analytic continuation as a method of phase determination. Physics Letters 35A: 259-260.

[62] Adachi T (2000) A new method for determining the phase in the x-ray diffraction structure analysis of phosphatidylcholine/alcohol. Chem Phys Lipids 107: 93–97.

[63] Katsaras J, Raghunathan VA, Dufourc EJ, Dufourcq J (1995) Evidence for a two-dimensional molecular lattice in subgel phase dppc bilayers. Biochemistry (Mosc) 34: 4684-4688.

[64] Raghunathan VA, Katsaras J (1995) Structure of the l_c' phase in a hydrated lipid multilamellar system. Phys Rev Lett 74: 4456–4459.

[65] Mills TT, Toombes GES, Tristram-Nagle S, Smilgies DM, Feigenson GW, et al. (2008) Order parameters and areas

in fluid-phase oriented lipid membranes using wide angle x-ray scattering. Biophys J 95: 669-681.

[66] Toppozini L, Armstrong CL, Barrett MA, Zheng S, Luo L, et al. (2012) Partitioning of ethanol into lipid membranes and its effect on fluidity and permeability as seen by x-ray and neutron scattering. Soft Matter 8: 11839-11849.

[67] Léonard A, Escrive C, Laguerre M, Pebay-Peyroula E, Néri W, et al. (2001) Location of cholesterol in dmpc membranes. a comparative study by neutron diffraction and molecular mechanics simulation. Langmuir 17: 2019–2030.

[68] Petrie RJ, Schnetkamp PP, Patel KD, Awasthi-Kalia M, Deans JP (2000) Transient translocation of the b cell receptor and src homology 2 domain-containing inositol phosphatase to lipid rafts: evidence toward a role in calcium regulation. J Immunol 165: 1220–1227.

[69] Papanikolaou A, Papafotika A, Murphy C, Papamarcaki T, Tsolas O, et al. (2005) Cholesterol-dependent lipid assemblies regulate the activity of the ecto-nucleotidase cd39. J Biol Chem 280: 26406–26414.

[70] Roth GJ, Stanford N, Majerus PW (1975) Acetylation of prostaglandin synthase by aspirin. Proc Natl Acad Sci USA 72: 3073–3076.

[71] Patrono C, García Rodríguez LA, Landolfi R, Baigent C (2005) Low-dose aspirin for the prevention of atherothrombosis. N Engl J Med 353: 2373–2383.

[72] Assadian A, Lax J, Meixner-Loicht U, Hagmüller GW, Bayer PM, et al. (2007) Aspirin resistance among long-term aspirin users after carotid endarterectomy and controls: flow cytometric measurement of aspirin-induced platelet inhibition. Journal of vascular surgery 45: 1142–1147.

[73] Frydman JNG, Fonseca AdSd, Rocha VCd, Benarroz MO, Rocha GdS, et al. (2010) Acetylsalicylic acid and morphology of red blood cells. Brazilian Archives of Biology and Technology 53: 575–582.

[74] Pereira-Leite C, Nunes C, Reis S (2013) Interaction of nonsteroidal anti-inflammatory drugs with membranes: *In vitro* assessment and relevance for their biological actions. Progress in lipid research 52: 571–584.

[75] Suwalsky M, Belmar J, Villena F, Gallardo MJ, Jemiola-Rzeminska M, et al. (2013) Acetylsalicylic acid (aspirin) and salicylic acid interaction with the human erythrocyte membrane bilayer induce *in vitro* changes in the morphology of erythrocytes. Archives of biochemistry and biophysics 539: 9–19.

[76] Sousa C, Nunes C, Lúcio M, Ferreira H, Lima JL, et al. (2008) Effect of nonsteroidal anti-inflammatory drugs on the cellular membrane fluidity. J Pharm Sci 97: 3195–3206.

[77] Shattil SJ, Cooper RA (1976) Membrane microviscosity and human platelet function. Biochemistry (Mosc) 15: 4832–4837.

[78] Gousset K, Wolkers WF, Tsvetkova NM, Oliver AE, Field CL, et al. (2002) Evidence for a physiological role for membrane rafts in human platelets. J Cell Physiol 190: 117–128.

[79] Padmavathi P, Reddy VD, Maturu P, Varadacharyulu N (2010) Smoking-induced alterations in platelet membrane fluidity and na+/k+-atpase activity in chronic cigarette smokers. J Atheroscler Thromb 17: 619–627.

[80] Tsuchiya H, Ohmoto S (2010) Comparative effects of b-carbolines on platelet aggregation and lipid membranes. Pharmacol Rep 62: 689–695.

[81] Nasedkin A, Davidsson J, Kumpugdee-Vollrath M (2013) Determination of nanostructure of liposomes containing two model drugs by x-ray scattering from a synchrotron source. Journal of synchrotron radiation 20: 0–0.

[82] Ong DS, Anzinger JJ, Leyva FJ, Rubin N, Addadi L, et al. (2010) Extracellular cholesterol-rich microdomains generated by human macrophages and their potential function in reverse cholesterol transport. Journal of lipid research 51: 2303–2313.

[83] Lúcio M, Nunes C, Gaspar D, Golebska K, Wisniewski M, et al. (2009) Effect of anti-inflammatory drugs in phosphatidylcholine membranes: A fluorescence and calorimetric study. Chemical Physics Letters 471: 300 - 309.

[84] Dies H, Toppozini L, Rheinstädter MC (2014) The interaction between amyloid-β peptides and anionic lipid membranes containing cholesterol and melatonin. Accepted for publication in PLOS ONE .